ACS APPLIED MATERIALS & INTERFACES

Research Article

www.acsami.org

Precipitation of PEG/Carboxyl-Modified Gold Nanoparticles with Magnesium Pyrophosphate: A New Platform for Real-Time Monitoring of Loop-Mediated Isothermal Amplification

Ailin Qin,[†] Lok Tin Fu,[†] Jacky K. F. Wong,[†] Li Yin Chau,[†] Shea Ping Yip,[‡] and Thomas M. H. Lee*[,†]

[†]Interdisciplinary Division of Biomedical Engineering, [‡]Department of Health Technology and Informatics, The Hong Kong Polytechnic University, Hung Hom, Kowloon, Hong Kong, China

Supporting Information

ABSTRACT: Gold nanoparticles have proven to be promising for decentralized nucleic acid testing by virtue of their simple visual readout and absorbance-based quantification. A major challenge toward their practical application is to achieve ultrasensitive detection without compromising simplicity. The conventional strategy of thermocycling amplification is unfavorable (because of both instrumentation and preparation of thermostable oligonucleotide-modified gold nanoparticle probes). Herein, on the basis of a previously unreported co-precipitation phenomenon between thiolated poly(ethylene glycol)/11-mercaptoundecanoic acid co-modified gold nanoparticles and magnesium pyrophosphate crystals (an isothermal DNA amplification reaction byproduct), a new ultrasensitive and simple DNA assay platform is developed. The binding mechanism underlying the co-precipitation phenomenon is found to be caused by the complexation of carboxyl and pyrophosphate with free magnesium ions. Remarkably, poly(ethylene glycol) does not hinder the binding and effectively stabilizes gold nanoparticles against magnesium ion-induced aggregation (without pyrophosphate). In fact, a similar phenomenon is observed in other poly(ethylene glycol)- and carboxyl-containing nanomaterials. When the gold nanoparticle probe is incorporated into a loop-mediated isothermal amplification reaction, it remains as a red dispersion for a negative sample (in the absence of a target DNA sequence) but appears as a red precipitate for a positive sample (in the presence of a target). This results in a first-of-its-kind gold nanoparticle-based DNA assay platform with isothermal amplification and real-time monitoring capabilities.

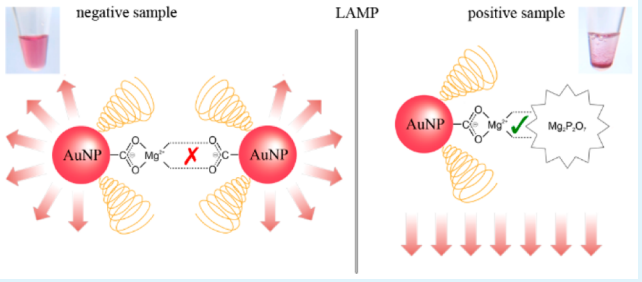

KEYWORDS: *DNA detection, isothermal amplification, real-time LAMP, gold nanoparticles, magnesium pyrophosphate, precipitation-based readout, point-of-care nucleic acid testing*

INTRODUCTION

The ability to perform nucleic acid testing in decentralized settings would bring tremendous benefits to medical diagnostics, food safety control, and environmental surveillance. By eliminating sample transportation to and queuing in central laboratories, timely treatment/response decisions can be made. Gold nanoparticle (AuNP)-based platforms are promising in view of their simple signal readout (visual interpretation or absorbance measurement). For nucleic acid detection, pioneered by Mirkin and co-workers,[1−3] two oligonucleotide-modified AuNP probes (each being complementary to half of a target sequence) are typically included. The two AuNP probes are dispersed in the absence of the target (the solution color appears red for 13 nm AuNPs; the surface plasmon resonance (SPR) absorption peak appears at 520 nm), but they are cross-linked/aggregated by the target (the solution color turns purple; red shift in SPR). Apart from cross-linking, alternative schemes based on non-cross-linking and salt-induced aggregation mechanisms are available.[4,5] The limits of detection (LODs) of these schemes are in the nanomolar range.

Over the past decade, tremendous efforts have been made to couple AuNP-based detection schemes with target amplification and signal amplification (such as target recycling), thereby achieving thousand- to billion-fold improvements in the LODs.[6−32] Nevertheless, most of these approaches required the separation of the detection step from the amplification step (i.e., postamplification open-tube addition of the AuNP probes), posing a high risk of carryover contamination. The incompatibility of the AuNP probes with the amplification step is due to two main factors: (1) particle aggregation, which occurs upon oligonucleotide desorption at temperatures higher than 70 °C and/or by ligand exchange (e.g., dithiothreitol) for oligonucleotide-modified AuNP probes prepared with a monothiol−gold linkage, and (2) enzyme inhibition, which occurs upon adsorption onto a AuNP surface for both oligonucleotide-modified and unmodified AuNPs. The ampli-

Received: January 2, 2017
Accepted: March 9, 2017
Published: March 9, 2017

DOI: 10.1021/acsami.7b00046
ACS Appl. Mater. Interfaces 2017, 9, 10472−10480

fication can be classified into thermocycling[6−17] (i.e., polymerase chain reaction and ligation chain reaction) and isothermal[18−32] methods. Several thermocycling-based closed-tube assay platforms were realized, with special strategies employed to enhance the thermal and chemical stabilities of the oligonucleotide-modified AuNP probes.[12−14] The need for thermocycling is nonetheless a drawback from an instrumentation point of view. To address this, isothermal amplification is highly desirable.[33] In a previous work, we developed a new type of AuNP probe for use in a closed-tube loop-mediated isothermal amplification (LAMP) assay.[27] LAMP operates at a constant temperature of 60−65 °C, generating a billion copies of a specific DNA sequence within 1 h.[34−36] Another favorable feature is the release of pyrophosphate ions ($P_2O_7^{4-}$) as a reaction byproduct, which complexes with magnesium ions (Mg^{2+}; enzyme cofactor) to form a precipitate (visible to the naked eye only under special lighting conditions).[35] We attempted to make use of Mg^{2+} and $P_2O_7^{4-}$ to trigger the aggregation and deaggregation of a AuNP probe (11-mercaptoundecanoic acid-modified AuNPs, MUA−AuNPs). When MUA−AuNPs were added into a LAMP reaction mixture, the complexation between Mg^{2+} and the carboxyl group (COO^-) of MUA resulted in particle aggregation and a concomitant color change from red to violet-blue. In the absence of the DNA target, a violet-blue precipitate was observed after LAMP. On the other hand, in the presence of the target, the $P_2O_7^{4-}$ that was generated formed a stronger complex with Mg^{2+} than COO^- and thus MUA−AuNPs were partially deaggregated (red-violet precipitate). This assay platform possesses the following advantages: it uses a cost-effective probe (MUA versus oligonucleotides with attachment chemistry modification), has simple temperature control, and permits ultrasensitive detection (LOD at the attomolar level). However, only qualitative results were obtained because the precipitated MUA−AuNPs, for both negative (without target) and positive (with target) samples throughout the LAMP reaction, did not facilitate real-time measurement.

In the present work, we report a new type of AuNP probe (co-modified with thiolated poly(ethylene glycol) and MUA, PEG/MUA−AuNPs) that exhibits totally different behavior in Mg^{2+} and $Mg_2P_2O_7$ than that of MUA−AuNPs, enabling real-time LAMP monitoring. PEG stabilizes the particles against Mg^{2+}-induced aggregation due to steric hindrance and therefore PEG/MUA−AuNPs (red color) remain dispersed in a negative LAMP sample. Remarkably, PEG/MUA−AuNPs bind effectively with $Mg_2P_2O_7$ in a positive LAMP sample, the co-precipitation of which results in a red precipitate. The progress of the LAMP reaction can then be monitored by measuring the absorbance of the supernatant. Such behavior is not unique to PEG/MUA−AuNPs; it resides in the surface functional groups, i.e., PEG and COO^-. In this regard, we show that PEG-modified graphene oxide (PEG−GO; GO contains COO^-) behaves almost identically to PEG/MUA−AuNPs. Another endeavor of this work is to develop a simple, hand-held, and low-cost prototype device for carrying out the real-time LAMP assay. The device is composed of three core modules: (1) heating by means of a disposable air-activated hand warmer powder; (2) absorbance measurement using a 520 nm laser diode, a photodiode, and supporting electronics (microcontroller board and battery); and (3) wireless signal transmission (Bluetooth), signal processing, and result display (smartphone).

EXPERIMENTAL SECTION

Materials Preparation and Characterization. AuNPs (14 nm in diameter) were synthesized based on the citrate reduction method.[37,38] The glassware and magnetic stir bar used for the synthesis were cleaned with aqua regia (mixture of concentrated hydrochloric acid and nitric acid in a volume ratio of 3:1), rinsed with water, and dried in an oven. *Aqua regia is harmful and highly corrosive; hence, it must be handled inside a fume hood and with adequate personal protective equipment.* All chemicals were purchased from Sigma-Aldrich unless otherwise specified. All aqueous solutions were prepared with ultrapure water from a Direct-Q 3 system (Millipore; 18.2 MΩ·cm; fitted with a Millipak Express 20 filter) unless otherwise specified. A solution of hydrogen tetrachloroaurate(III) (50 mL, 0.01 wt %) was boiled under reflux with vigorous stirring. Then, sodium citrate (5 mL, 1 wt %) was added quickly. The solution color changed from pale yellow to deep red within several minutes. Heating and stirring were continued for 10 min, followed by cooling to room temperature under stirring. The AuNP solution was stored at 4 °C until use. The size and concentration of the AuNPs were determined according to the method established by Haiss and co-workers based on UV−visible absorbance measurements.[39] UV−visible spectra were acquired using an Ultrospec 2100 pro UV/visible spectrophotometer (GE Healthcare).

For the preparation of PEG/MUA−AuNPs, MUA−AuNPs, and PEG−AuNPs, the as-synthesized AuNP solution was concentrated by centrifuging at 5800 rpm for 45 min (centrifuge 5415 D, Eppendorf), removing the supernatant, and redispersing with ultrapure DNase/RNase-free distilled water (Invitrogen; one-tenth of the original volume). Stock solutions of thiolated PEG (Laysan Bio; M_r of 2000 Da; 10 mM; ultrapure DNase/RNase-free distilled water), MUA (10 mM in dimethyl sulfoxide), phosphate buffer (0.1 M, pH 7.4; ultrapure DNase/RNase-free distilled water), and Tween 20 (1 mg/mL; ultrapure DNase/RNase-free distilled water) were freshly prepared. For PEG/MUA−AuNPs (PEG-to-MUA molar ratio of 2:1), AuNPs (20 nM), thiolated PEG (0.1 mM), MUA (50 μM), phosphate buffer (5 mM), and Tween 20 (10 μg/mL) were mixed (total volume of 400 μL) and incubated for 24 h under shaking at 1400 rpm. PEG/MUA−AuNPs with a 1:10 PEG-to-MUA molar ratio were prepared with 0.1 mM thiolated PEG and 1 mM MUA, and PEG/MUA−AuNPs with a 40:1 PEG-to-MUA molar ratio were prepared with 2 mM thiolated PEG and 50 μM MUA. The preparation of MUA−AuNPs and PEG−AuNPs was similar to that of PEG/MUA−AuNPs except that thiolated PEG was not used for the former and MUA was not used for the latter. The PEG/MUA−AuNP, MUA−AuNP, and PEG−AuNP solutions were stored at room temperature until use. UV−visible spectra of the synthesized PEG/MUA−AuNPs were acquired using an Ultrospec 2100 pro UV/visible spectrophotometer.

GO (carboxyl graphene water dispersion) and pyrene−PEG (M_r of 2000 Da) were purchased from ACS Material and Creative PEGWorks, respectively. PEG−GO was prepared by incubating GO (0.5 mg/mL), pyrene−PEG (10 mg/mL), and NaCl (0.154 M) at room temperature for 1 h. Then, centrifugation (13 200 rpm for 1 h) was performed to remove excess pyrene−PEG, and the PEG−GO thus obtained was redispersed in water.

Precipitation Tests with $Mg_2P_2O_7$. To test the effects of Mg^{2+} and $Mg_2P_2O_7$ on PEG/MUA−AuNPs, a 14 μL mixture comprising 2 μL of 10× isothermal amplification buffer (New England BioLabs; 200 mM Tris-HCl, 100 mM $(NH_4)_2SO_4$, 500 mM KCl, 20 mM $MgSO_4$, and 1% Tween 20), 1.6 μL of 25 mM $MgCl_2$ (New England BioLabs), and 0.28 μL of 100 mM $K_4P_2O_7$ (only for the sample with $Mg_2P_2O_7$) was first prepared (the volume was adjusted with water), followed by the addition of 6 μL of 20 nM PEG/MUA−AuNPs and then incubation at 65 °C (GeneAmp PCR system 9700, Applied Biosystems) or room temperature for 1 h. The final concentrations of Mg^{2+}, $P_2O_7^{4-}$, and PEG/MUA−AuNPs were 4 mM, 1.4 mM, and 6 nM, respectively. Similar experiments were carried out with MUA−AuNPs and PEG−AuNPs (6 nM), as well as GO and PEG−GO (50 μg/mL). The samples with MUA−AuNPs were subjected to mild sonication for 10 s after the incubation step. Another set of experiments was included by performing the incubation step (i.e.,

DOI: 10.1021/acsami.7b00046
ACS Appl. Mater. Interfaces 2017, 9, 10472−10480

forming $Mg_2P_2O_7$ crystals) before the addition of PEG/MUA–AuNPs and MUA–AuNPs, followed by further incubation at room temperature for 1 h. Yet another set of experiments was included to remove free Mg^{2+} from the formed $Mg_2P_2O_7$ crystals before the addition of PEG/MUA–AuNPs and MUA–AuNPs (centrifuged at 4000 rpm for 30 s, removed the supernatant, and redispersed in 14 μL of water). Additionally, for PEG/MUA–AuNPs, an experiment was carried out by substituting $K_4P_2O_7$ with dNTPs (New England BioLabs; final concentration of 1.4 mM total or 0.35 mM each).

Samples of MUA–AuNPs, PEG/MUA–AuNPs, $Mg_2P_2O_7$, MUA–AuNPs with $Mg_2P_2O_7$ (crystals formed before the addition of MUA–AuNPs), and PEG/MUA–AuNPs with $Mg_2P_2O_7$ (crystals formed before the addition of PEG/MUA–AuNPs) were characterized by Fourier transform infrared (FTIR) spectroscopy. The samples were dried in a vacuum oven overnight (each sample was prepared from three identical tubes as described in the previous paragraph). FTIR spectra were acquired in transmission mode using the KBr pellet method (Nicolet iS 50 FT-IR spectrometer, Thermo Scientific).

LAMP. Six primers were used for amplifying lambda DNA according to previously published sequences:[36] FIP: 5′-CAGCCAGCCGCAGCACGTTCGCTCATAGGAGATATGGTAGAGCCGC-3′; BIP: 5′-GAGAGAATTTGTACCACCTCCCACCGGGCACATAGCAGTCCTAGGGACAGT-3′; F3: 5′-GGCTTGGCTCTGCTAACACGTT-3′; B3: 5′-GGACGTTTGTAATGTCCGCTCC-3′; loop F: 5′-CTGCATACGACGTGTCT-3′; and loop B: 5′-ACCATCTATGACTGTACGCC-3′. The primers were purchased from Integrated DNA Technologies (HPLC-purified). Other LAMP reagents were purchased from New England BioLabs unless otherwise specified. All solutions were prepared with ultrapure DNase/RNase-free distilled water. A 20 μL mixture comprising 1× isothermal amplification buffer (20 mM Tris-HCl, 10 mM $(NH_4)_2SO_4$, 50 mM KCl, 2 mM $MgSO_4$, 0.1% Tween 20, pH 8.8), FIP (0.8 μM), BIP (0.8 μM), F3 (0.2 μM), B3 (0.2 μM), loop F (0.4 μM), loop B (0.4 μM), lambda DNA (100 000 copies for a positive sample, and 0 copies for a negative sample), dNTPs (1.4 mM total or 0.35 mM each unless otherwise specified), Bst 2.0 DNA polymerase (0.32 units/μL), betaine (1 M; Sigma-Aldrich), and PEG/MUA–AuNPs (6 nM) was incubated at 65 °C for 1 h (GeneAmp PCR system 9700). Parallel experiments were carried out without PEG/MUA–AuNPs, with MUA–AuNPs, or with PEG–AuNPs. The samples with MUA–AuNPs were subjected to mild sonication for 10 s after the LAMP reaction.

The samples described in the previous paragraph were characterized by transmission electron microscopy (TEM). After the LAMP reaction, the samples were centrifuged at 5800 rpm for 10 min and redispersed in water (repeated three times). Then, the samples (2 μL) were applied onto carbon-coated copper grids, dried under ambient conditions, and examined using a JEM-2100F field emission electron microscope (JEOL).

For specificity evaluation, four different template combinations of lambda DNA (specific template) and pBR322 DNA (nonspecific template) were included. In addition to performing a visual readout, the LAMP reaction products were analyzed by agarose gel electrophoresis. Mixtures of the products (8 μL) and gel loading buffer (BlueJuice, Invitrogen), together with a DNA ladder (low molecular weight DNA ladder, New England BioLabs), were loaded into an agarose gel (2 wt % in 0.5× TBE buffer: 45 mM Tris, 45 mM boric acid, 1 mM EDTA, pH 8.0) and subjected to electrophoresis at 120 V for 1.5 h. Then, the gel was stained with ethidium bromide (0.5 μg/mL) for 10 min and visualized by a Gel Doc XR+ System (Bio-Rad). For LOD determination, different amounts of the lambda DNA template were tested (0 to 100 000 copies). The amplification results were checked by visual readout, agarose gel electrophoresis analysis, and absorbance measurement. Quantification by absorbance measurement was performed at 10 min intervals. The samples were centrifuged at 4000 rpm for 30 s, the supernatants (14 μL) were collected and diluted with water (56 μL), and the absorbance at 520 nm was measured using an Ultrospec 2100 pro UV/visible spectrophotometer.

Homemade Prototype Device for Real-Time LAMP Assay. Holders for the sample tubes together with the heating powder, two laser diodes, and two photodiodes and their alignment were drawn using SOLIDWORKS 3D CAD software. They were fabricated by a Fortus 400mc 3D printer (Stratasys) using acrylonitrile butadiene styrene. Two 520 nm lasers (HH-520-5) were purchased from the 1688 web store, and two photodiodes (TSL250R-LF) were purchased from RS Components. Two Arduino Uno boards were purchased from Arduino, and one Bluetooth module (HC-05) was purchased from the Taobao web store. Simple output control was encoded into the Arduino boards with the Arduino software platform. All device components were housed within an acrylic case. An Android application was developed with Android Studio and installed in a smartphone to receive, process, and display the signals from the photodiodes via the Bluetooth module.

To perform the real-time LAMP assay with the homemade device, LAMP reaction mixtures were prepared identically to those mentioned in the previous section, except that 15 μL of silicone oil was added to prevent evaporation. Heating powder was prepared by mixing fresh (5.5 g) and used (20 g) powders (Nukupon, Kokubo). The mixed powder was immediately loaded into the sample tubes and heating powder holder. It took ∼10 min for the heating powder to reach 60 °C (determined from the time point at which the fresh powder was exposed to ambient air; monitored by a digital multimeter, UT33C, Uni-Trend). Then, the sample tubes were inserted into the holder. The device was turned on and paired to the smartphone to start the measurement.

RESULTS AND DISCUSSION

Precipitation Tests with $Mg_2P_2O_7$. PEG/MUA–AuNPs were prepared by coassembly of thiolated PEG (M_r of 2000 Da) and MUA onto 14 nm AuNPs. The surface modification caused only a slight red shift of the SPR absorption peak (524 nm) compared with that of unmodified AuNPs (520 nm), as shown in Figure S1 (Supporting Information). This work was based on the remarkable observation that PEG/MUA–AuNPs remained dispersed in Mg^{2+} (red solution; 4 mM Mg^{2+}) but precipitated with $Mg_2P_2O_7$ crystals (red precipitate; 4 mM Mg^{2+} and 1.4 mM $K_4P_2O_7$) after incubation at 65 °C for 1 h (Figure 1b). These conditions simulated the negative and positive reactions in LAMP, suggesting the feasibility of monitoring the progress of a LAMP reaction in real-time by

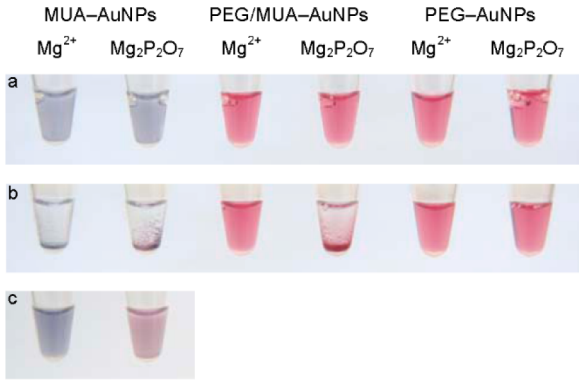

Figure 1. Photographs showing the effects of magnesium ions (Mg^{2+}) and magnesium pyrophosphate ($Mg_2P_2O_7$) on 11-mercaptoundecanoic acid-modified gold nanoparticles (MUA–AuNPs), thiolated poly(ethylene glycol) and 11-mercaptoundecanoic acid-modified gold nanoparticles (PEG/MUA–AuNPs), and thiolated poly(ethylene glycol)-modified gold nanoparticles (PEG–AuNPs). The concentrations of Mg^{2+}, $Mg_2P_2O_7$, and the three types of AuNPs were 4 mM, 1.4 mM (4 mM Mg^{2+} and 1.4 mM $K_4P_2O_7$), and 6 nM, respectively. (a) Before and (b) after incubation at 65 °C for 1 h. (c) The two MUA–AuNPs samples in (b) were subjected to mild sonication for 10 s after the incubation step.

DOI: 10.1021/acsami.7b00046
ACS Appl. Mater. Interfaces 2017, 9, 10472–10480

Scheme 1. Interactions of MUA–AuNP and PEG/MUA–AuNP with Mg^{2+} and $Mg_2P_2O_7$ Crystals (with and without Free Mg^{2+})[a]

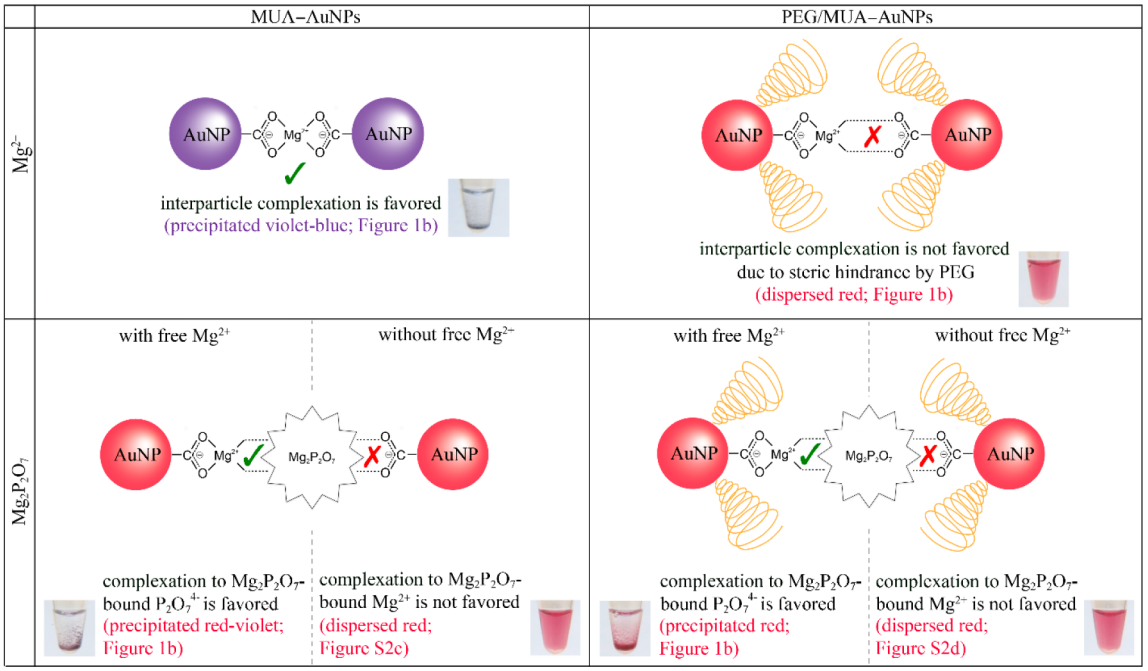

[a]The structures are not drawn to scale (AuNP: 14 nm; $Mg_2P_2O_7$ crystal: ~1 μm).

measuring the absorbance of the supernatant at 520 nm. It should be pointed out that the co-precipitation rate was temperature-dependent, with a slower rate at a lower temperature (at room temperature, it took 2 h for complete co-precipitation; data not shown). When AuNPs were modified with either MUA (MUA–AuNPs) or thiolated PEG (PEG–AuNPs), the results were completely different (Figure 1b). For MUA–AuNPs, violet-blue and red-violet precipitates were observed with Mg^{2+} and $Mg_2P_2O_7$, respectively. In a previous work, we made use of this difference to realize an end-point colorimetric LAMP assay platform.[27] The samples were redispersed by sonication to make result interpretation easier (Figure 1c). In fact, when MUA–AuNPs were added to Mg^{2+} as well as Mg^{2+} and $K_4P_2O_7$ (Mg^{2+} in excess), the solution color changed from red to violet-blue instantaneously as a result of the complexation between Mg^{2+} and COO^- (Figure 1a; the red state in the absence of Mg^{2+} is not shown). Then, the violet-blue aggregates gradually precipitated. During the thermal incubation step, for the sample with Mg^{2+} and $K_4P_2O_7$, $Mg_2P_2O_7$ crystals were formed, extracting Mg^{2+} from the aggregates; thus, the precipitate turned red-violet (presumably due to partial deaggregation). However, it was unclear why the deaggregated MUA–AuNPs remained precipitated. To reveal the exact mechanism, herein, experiments were performed to study the interaction between MUA–AuNPs and $Mg_2P_2O_7$ crystals, as well as the effect of free Mg^{2+} on such an interaction. Figure S2a shows that the solution color was red instead of violet-blue when MUA–AuNPs were added to Mg^{2+} and $K_4P_2O_7$ (Mg^{2+} in excess) after the thermal incubation step (i.e., $Mg_2P_2O_7$ crystals were first formed). This indicates that the Mg^{2+}-induced aggregation of MUA–AuNPs no longer occurred. Moreover, the eventual formation of a red precipitate (Figure S2b) suggests the binding of MUA–AuNPs to $Mg_2P_2O_7$ crystals. We hypothesized that the interaction involved the complexation of COO^- and $P_2O_7^{4-}$ with free Mg^{2+}. To test this, the formed $Mg_2P_2O_7$ crystals were centrifuged to remove free Mg^{2+} before adding MUA–AuNPs. Without free Mg^{2+}, MUA–AuNPs remained dispersed (Figure S2c). For PEG/MUA–AuNPs, after the addition of Mg^{2+} and thermal incubation, the solution remained as a red dispersion (Figures 1a,b). Steric hindrance by PEG effectively stabilized the particles against Mg^{2+}-induced aggregation. On the other hand, PEG did not hinder the binding between PEG/MUA–AuNPs and $Mg_2P_2O_7$ crystals (a red precipitate resulted after thermal incubation; Figure 1b). The binding interaction was analogous to that of MUA–AuNPs, i.e., complexation of COO^- and $P_2O_7^{4-}$ with free Mg^{2+}. This was again supported by the formation of a red dispersion without free Mg^{2+} (Figure S2d). With $Mg_2P_2O_7$ crystals as the binding site, the steric hindrance by PEG was rendered ineffective (in contrast with the case with PEG on both sides of the AuNPs). Illustrations of the interactions of MUA–AuNP and PEG/MUA–AuNP with Mg^{2+} and $Mg_2P_2O_7$ crystals (with and without free Mg^{2+}) are presented in Scheme 1. For PEG–AuNPs, no co-precipitation was observed with $Mg_2P_2O_7$ (red dispersion; Figure 1b), further confirming the crucial role of COO^- in the binding. Not surprisingly, the amounts of PEG and MUA during the preparation of PEG/MUA–AuNPs had a significant impact on the resulting behavior. The optimum PEG-to-MUA molar ratio was 2:1 (Figure S3; a lower ratio behaved like MUA–AuNPs and a higher ratio behaved like PEG–AuNPs). Figure S4 shows the FTIR spectra of $Mg_2P_2O_7$, MUA–AuNPs with $Mg_2P_2O_7$, and PEG/MUA–AuNPs with $Mg_2P_2O_7$. The characteristic bands of $Mg_2P_2O_7$ were evident (P═O stretch: 1300–1000 cm^{-1}; P–O–P stretch: 975–860 cm^{-1}; O–P–O bend: 640–545 cm^{-1}). Interestingly, the binding of MUA–AuNPs had a negligible effect on the characteristic bands of $Mg_2P_2O_7$, whereas the binding of PEG/MUA–AuNPs caused a significant diminution in the intensity of the bands. This might be attributed to a certain interaction between PEG and $P_2O_7^{4-}$,

DOI: 10.1021/acsami.7b00046
ACS Appl. Mater. Interfaces 2017, 9, 10472–10480

which is facilitated only after the binding between PEG/MUA–AuNPs and $Mg_2P_2O_7$ (complexation of COO^- and $P_2O_7^{4-}$ with free Mg^{2+}).

It should be highlighted that the dispersion of PEG/MUA–AuNPs with Mg^{2+} and the co-precipitation with $Mg_2P_2O_7$ were controlled by PEG, COO^-, $P_2O_7^{4-}$, and free Mg^{2+}. The key function of AuNPs was to enable a clear visual readout. We reasoned that this strategy could be applied to other nanomaterials containing PEG and COO^-. To test this, GO was selected (brown in color) and modified with PEG (PEG–GO) using pyrene–PEG (π-stacking interaction between pyrene and GO[40,41]). Upon the addition of Mg^{2+} as well as Mg^{2+} and $K_4P_2O_7$, PEG–GO was dispersed (Figure 2a; brown

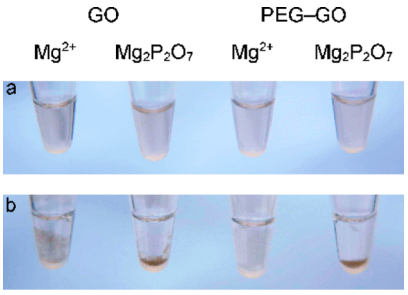

Figure 2. Photographs showing the effects of Mg^{2+} and $Mg_2P_2O_7$ on graphene oxide (GO) and pyrene–poly(ethylene glycol)-modified GO (PEG–GO). The concentrations of Mg^{2+}, $Mg_2P_2O_7$, and GO/PEG–GO were 4 mM, 1.4 mM (4 mM Mg^{2+} and 1.4 mM $K_4P_2O_7$), and 50 μg/mL, respectively. (a) Before and (b) after incubation at 65 °C for 1 h.

dispersion). After thermal incubation, the sample with Mg^{2+} remained dispersed, whereas the sample with $Mg_2P_2O_7$ appeared as a brown precipitate (Figure 2b); this is consistent with the results for PEG/MUA–AuNPs. The behavior of GO was also studied (in the same manner as the comparison between PEG/MUA–AuNPs and MUA–AuNPs). For GO, the complexation between Mg^{2+} and COO^- resulted in mild precipitation (Figure 2b). This implies that the extent of aggregation was less severe with GO than with MUA–AuNPs, which depends on the density of COO^-. One minor point to note is that, unlike AuNPs, the aggregation of GO did not involve a color change. With $Mg_2P_2O_7$, GO was well-precipitated.

LAMP. Aside from $Mg_2P_2O_7$-induced precipitation, another prerequisite for monitoring LAMP with PEG/MUA–AuNPs is the inability of all reaction components to trigger precipitation, particularly deoxynucleoside triphosphates (dNTPs; precursor of $P_2O_7^{4-}$). As shown in Figure S5, PEG/MUA–AuNPs remained dispersed with dNTPs after thermal incubation. Next, the main task was to demonstrate a complete assay for the differentiation between negative (the absence of a specific DNA template) and positive (the presence of a specific DNA template) samples. The specific template used in this work was lambda DNA. Figure 3a shows that the LAMP reaction mixtures containing PEG/MUA–AuNPs appeared as red dispersions before thermal incubation. After a 1 h incubation at 65 °C, as shown in Figure 3b, the negative sample remained dispersed, whereas the positive sample (with 100 000 copies; 8 fM in a reaction volume of 20 μL) appeared as a red precipitate. It should be noted that the concentration of dNTPs (1.4 mM total or 0.35 mM each) was optimized to achieve complete/nearly complete precipitation of PEG/MUA–AuNPs in the

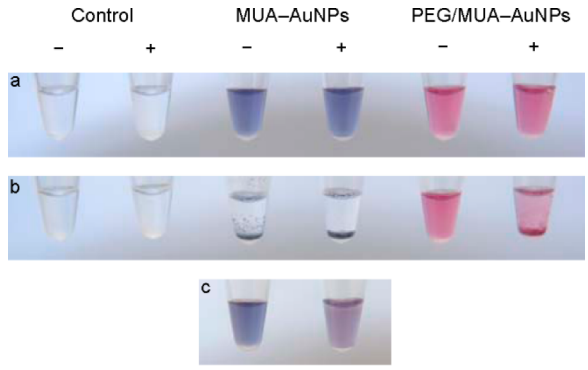

Figure 3. Loop-mediated isothermal amplification (LAMP) assay: (two left columns, four tubes) control without AuNPs; (two middle columns, six tubes) with MUA–AuNPs; and (two right columns, four tubes) with PEG/MUA–AuNPs. Negative samples ("–" columns) contained no lambda DNA target, whereas positive samples ("+" columns) contained 100 000 copies of lambda DNA target. (a) Before and (b) after incubation at 65 °C for 1 h. (c) The two MUA–AuNP samples in (b) were subjected to mild sonication for 10 s after the incubation step.

positive sample (Figure S6). With 2 mM Mg^{2+} (standard concentration in 1× isothermal amplification buffer), a lower concentration of dNTPs (half of the optimum one) resulted in incomplete precipitation (less $Mg_2P_2O_7$ crystals were formed), whereas a higher concentration of dNTPs (double the optimum one) resulted in no precipitation (no free Mg^{2+} due to the excess dNTPs). Experiments were also carried out without AuNPs, with MUA–AuNPs, or with PEG–AuNPs to better illustrate the advantage of PEG/MUA–AuNPs (Figures 3 and S7a). Without AuNPs, under ambient light conditions, it was very difficult to discern the white precipitate in the positive sample. With MUA–AuNPs, the negative (violet-blue precipitate) and positive (red-violet precipitate) samples were distinguishable only after mild sonication. With PEG–AuNPs, there was no difference between the negative and positive samples (red dispersions in both cases). These reaction products were further analyzed by TEM. In all of the positive samples, $Mg_2P_2O_7$ crystals were formed (size ~ 1 μm; likely to be clusters of platelets and needles;[42] Figures 4b,d,f and S7c). Another important aspect was the different behavior of the three types of AuNPs: MUA–AuNPs were bound to the $Mg_2P_2O_7$ crystals in a partially aggregated manner (more precisely, partially deaggregated as compared with those in the negative sample; Figures 4c,d), PEG/MUA–AuNPs were bound to the $Mg_2P_2O_7$ crystals in a dispersed manner (Figure 4f), and PEG–AuNPs were not bound to the $Mg_2P_2O_7$ crystals (Figure S7c).

The performance of the assay in terms of specificity, dynamic range, and LOD was then assessed. For specificity evaluation, lambda DNA and pBR322 DNA were used as specific and nonspecific templates, respectively. Figure 5a shows that the sample containing the nonspecific template (100 000 copies) remained as a red dispersion, just like the sample without both templates. Moreover, the samples containing only the specific template as well as both the specific and nonspecific templates appeared as red precipitates. The amplification results were confirmed by agarose gel electrophoresis analysis of the reaction products (Figure S8). As expected, characteristic ladder-like LAMP products were observed only in samples containing the specific templates. It should be pointed out that the results were similar to those of the controls without PEG/

DOI: 10.1021/acsami.7b00046
ACS Appl. Mater. Interfaces 2017, 9, 10472–10480

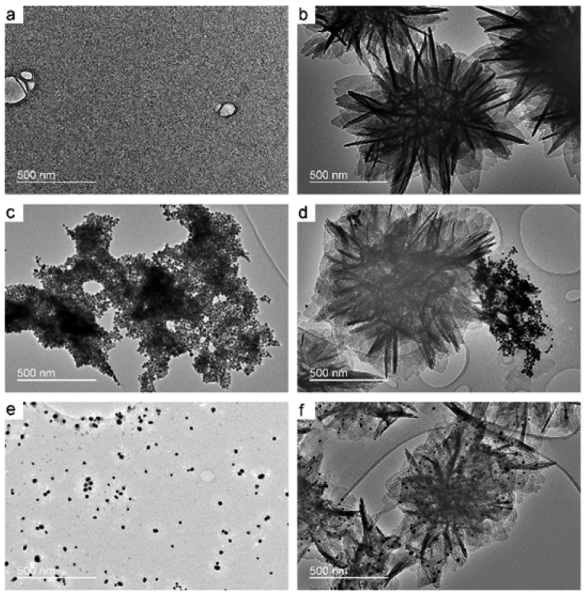

Figure 4. Transmission electron microscopy (TEM) photographs of the LAMP reaction products in Figure 3b: (a) negative sample without AuNPs, (b) positive sample without AuNPs, (c) negative sample with MUA–AuNPs, (d) positive sample with MUA–AuNPs, (e) negative sample with PEG/MUA–AuNPs, and (f) positive sample with PEG/MUA–AuNPs.

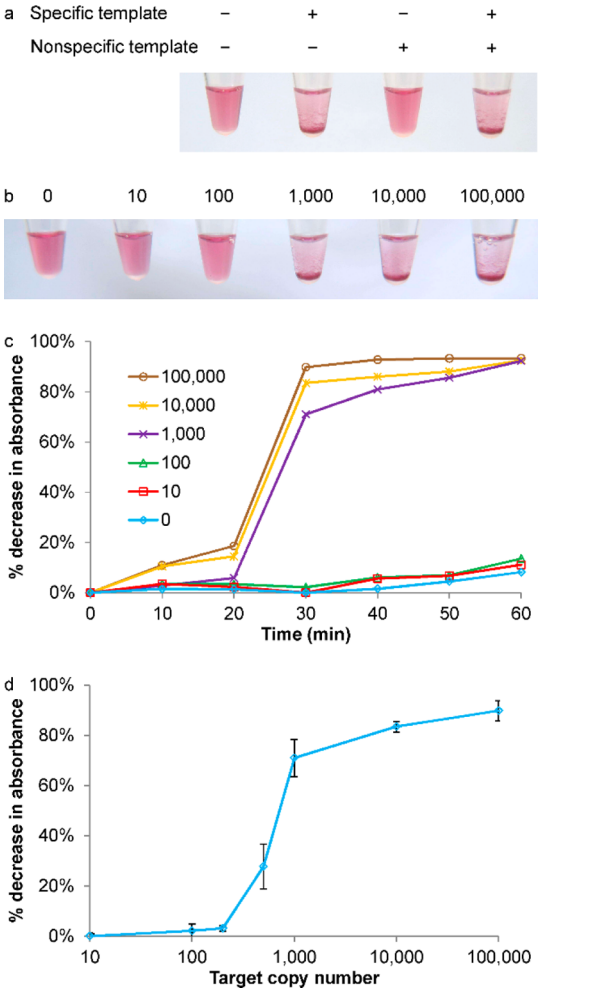

Figure 5. Specificity and sensitivity of the LAMP assay with PEG/MUA–AuNPs. (a) Photograph showing the amplification results of four different template combinations of lambda DNA (specific template) and pBR322 DNA (nonspecific template): (from left to right) sample without template, sample with lambda DNA, sample with pBR322 DNA, and sample with lambda DNA and pBR322 DNA. The copy number of both templates was 100 000. Photograph showing the amplification results of different copy numbers of lambda DNA target (0 to 100 000 copies) at a reaction time of 1 h. (c) Plots of percentage decrease in absorbance versus LAMP reaction time for the samples in (b). (d) Plot of percentage decrease in absorbance versus target copy number at a reaction time of 30 min (the corresponding photograph is given in Figure S10). The error bars represent the standard deviation of three measurements.

MUA–AuNPs, illustrating the excellent compatibility of PEG/MUA–AuNPs with LAMP. For dynamic range and LOD determination, different amounts of lambda DNA (0 to 100 000 copies) were tested. Figure 5b shows that the samples with 100 copies or less of lambda DNA appeared as red dispersions, whereas the samples with 1000 copies or more appeared as red precipitates. The amplification results were again confirmed by agarose gel electrophoresis analysis (Figure S9). The precipitation process was monitored by measuring the absorbance of the supernatant at 10 min intervals (520 nm; the samples were briefly centrifuged to remove the formed $Mg_2P_2O_7$ crystals along with the bound PEG/MUA–AuNPs). As shown in Figure 5c, for the samples with 1000 copies or more of lambda DNA, there was a sharp change in the absorbance from 20 to 30 min. A calibration plot of absorbance change versus target copy number with a reaction time of 30 min is given in Figure 5d (a photograph of the samples is given in Figure S10), indicating a dynamic range of more than 2 orders of magnitude and an LOD of 500 copies (~40 aM; reaction volume of 20 μL).

Homemade Prototype Device for Real-Time LAMP Assay. To demonstrate the applicability of the developed assay scheme for decentralized DNA testing, a simple, palm-sized, and low-cost prototype device was built to provide the two essential elements: a reaction temperature of 60–65 °C (achieved using a disposable air-activated hand warmer powder) and the ability to measure the absorbance in real-time (520 nm laser diode, photodiode, and supporting electronics). Several plastic parts were specially designed to hold two sample tubes together with heating powder, two laser diodes, and two photodiodes (Figure 6a). These parts were fabricated by 3D printing and assembled using an alignment holder. The sample tubes and heating powder holder had two important features: (1) a small channel (cross-sectional area of 1.5 mm^2) to direct the light beam through the sample (at half-height) and (2) the bottom portion of the sample tube (i.e., up to the height of the LAMP reaction mixture) was in contact with the heating powder (except for the area occupied by the light beam channel). The two laser diodes were controlled by one Arduino Uno microcontroller board, and the two photodiodes as well as a Bluetooth module were controlled by another Arduino Uno microcontroller board. Each board was powered by a 9 V battery. The signals from the photodiodes were sent wirelessly via Bluetooth to a smartphone for data processing and result display (self-developed Android application). Figure S11 shows that the temperature of the heating powder was maintained between 60 and 65 °C for 1 h, providing the optimum conditions for the LAMP reaction. Figure 6b presents the signal–time plots of the samples containing 10 000 and 100 000 copies of lambda DNA using

DOI: 10.1021/acsami.7b00046
ACS Appl. Mater. Interfaces 2017, 9, 10472–10480

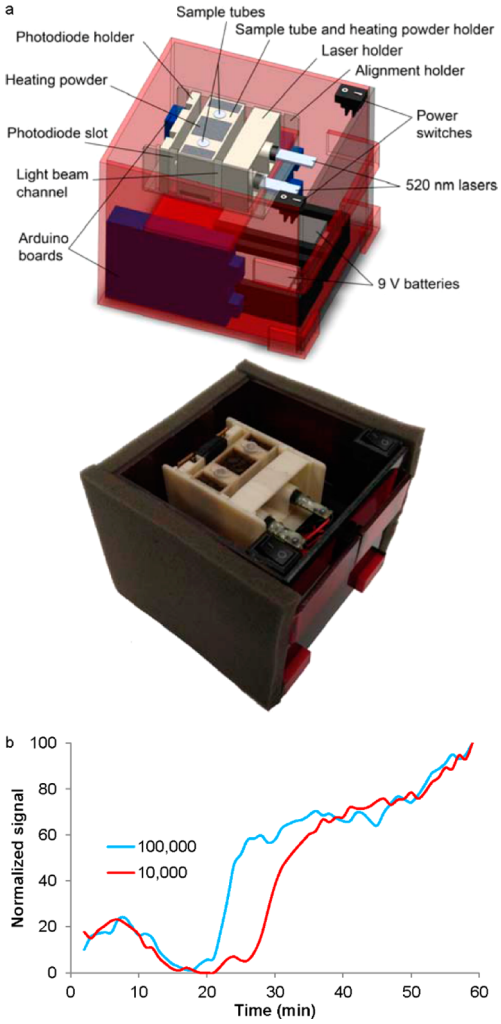

Figure 6. Homemade prototype device for real-time LAMP assay. (a) Schematic (top) and photograph (bottom) of the homemade prototype device. (b) Plots of photodiode signal versus LAMP reaction time using the homemade prototype device for samples containing 10 000 and 100 000 copies of lambda DNA target.

the homemade prototype device, which are consistent with the results using a benchtop dry block heater and UV−visible spectrophotometer (end-point detection of the supernatant after centrifugation; Figure 5c).

CONCLUSIONS

We showed that PEG/MUA−AuNPs and PEG−GO, both containing PEG and COO^-, were dispersed in Mg^{2+} but precipitated in $Mg_2P_2O_7$. PEG served as an effective stabilizer against Mg^{2+}-induced aggregation of COO^--containing AuNPs or GO, yet it permitted their binding to $Mg_2P_2O_7$ crystals (complexation of COO^- and $P_2O_7^{4-}$ with free Mg^{2+}). We made use of these properties to achieve real-time monitoring of a LAMP assay using PEG/MUA−AuNPs. This assay platform is highly specific, ultrasensitive (down to 500 copies, ~40 aM), rapid (30 min), and carryover contamination-free (closed-tube). We also developed a simple, palm-sized, and low-cost prototype device to perform the assay. Although only purified DNA templates were tested in the present work, LAMP has proven to be highly tolerant of unpurified samples.[43,44] Taken together, our platform is readily applicable to decentralized DNA testing. We believe that the dispersion/precipitation mechanism depicted here can be applied to other types of nanomaterials, thereby extending beyond visual/absorbance-based readouts, e.g., semiconductor and graphene quantum dots with a fluorescence readout. Another potential extension of the current platform is to replace PEG with alternative stabilizers.

ASSOCIATED CONTENT

Supporting Information

The Supporting Information is available free of charge on the ACS Publications website at DOI: 10.1021/acsami.7b00046.

Visible absorption spectra of AuNPs and PEG/MUA−AuNPs; effects of Mg^{2+} and $Mg_2P_2O_7$ on MUA−AuNPs and PEG/MUA−AuNPs; effects of Mg^{2+} and $Mg_2P_2O_7$ on PEG/MUA−AuNPs with different PEG-to-MUA molar ratios; FTIR spectra of MUA−AuNPs, PEG/MUA−AuNPs, $Mg_2P_2O_7$, MUA−AuNPs with $Mg_2P_2O_7$, and PEG/MUA−AuNPs with $Mg_2P_2O_7$; effect of dNTPs on PEG/MUA−AuNPs; effects of dNTPs concentration on LAMP assay with PEG/MUA−AuNPs; LAMP assay with PEG−AuNPs; agarose gel electrophoretograms of the LAMP reaction products in the specificity and sensitivity tests with PEG/MUA−AuNPs; photograph showing the LAMP results of different copy numbers of lambda DNA target at 30 min reaction time with PEG/MUA−AuNPs; and plot of temperature versus time of the disposable air-activated hand warmer powder used in the homemade prototype device for the real-time LAMP assay (PDF)

AUTHOR INFORMATION

Corresponding Author

*E-mail: ming-hung.lee@polyu.edu.hk.

ORCID

Thomas M. H. Lee: 0000-0003-3950-0232

Author Contributions

The manuscript was written through contributions of all authors. All authors have given approval to the final version of the manuscript.

Notes

The authors declare no competing financial interest.

ACKNOWLEDGMENTS

This work was supported by the General Research Fund from the Research Grants Council of Hong Kong (project number PolyU 501413) and the Central Research Grant from The Hong Kong Polytechnic University (project numbers G-YBRU and G-YBFH).

REFERENCES

(1) Mirkin, C. A.; Letsinger, R. L.; Mucic, R. C.; Storhoff, J. J. A DNA-Based Method for Rationally Assembling Nanoparticles into Macroscopic Materials. *Nature* **1996**, *382*, 607−609.

(2) Elghanian, R.; Storhoff, J. J.; Mucic, R. C.; Letsinger, R. L.; Mirkin, C. A. Selective Colorimetric Detection of Polynucleotides Based on the Distance-Dependent Optical Properties of Gold Nanoparticles. *Science* **1997**, *277*, 1078−1081.

(3) Storhoff, J. J.; Elghanian, R.; Mucic, R. C.; Mirkin, C. A.; Letsinger, R. L. One-Pot Colorimetric Differentiation of Polynucleotides with Single Base Imperfections Using Gold Nanoparticle Probes. *J. Am. Chem. Soc.* **1998**, *120*, 1959−1964.

DOI: 10.1021/acsami.7b00046
ACS Appl. Mater. Interfaces 2017, 9, 10472−10480

(4) Sato, K.; Hosokawa, K.; Maeda, M. Rapid Aggregation of Gold Nanoparticles Induced by Non-Cross-Linking DNA Hybridization. *J. Am. Chem. Soc.* **2003**, *125*, 8102−8103.
(5) Li, H.; Rothberg, L. Colorimetric Detection of DNA Sequences Based on Electrostatic Interactions with Unmodified Gold Nanoparticles. *Proc. Natl. Acad. Sci. U. S. A.* **2004**, *101*, 14036−14039.
(6) Li, H.; Rothberg, L. J. Label-Free Colorimetric Detection of Specific Sequences in Genomic DNA Amplified by the Polymerase Chain Reaction. *J. Am. Chem. Soc.* **2004**, *126*, 10958−10961.
(7) Sato, K.; Hosokawa, K.; Maeda, M. Non-Cross-Linking Gold Nanoparticle Aggregation as a Detection Method for Single-Base Substitutions. *Nucleic Acids Res.* **2005**, *33*, e4.
(8) Li, J.; Chu, X.; Liu, Y.; Jiang, J.-H.; He, Z.; Zhang, Z.; Shen, G.; Yu, R.-Q. A Colorimetric Method for Point Mutation Detection Using High-Fidelity DNA Ligase. *Nucleic Acids Res.* **2005**, *33*, e168.
(9) Jung, Y. L.; Jung, C.; Parab, H.; Li, T.; Park, H. G. Direct Colorimetric Diagnosis of Pathogen Infections by Utilizing Thiol-Labeled PCR Primers and Unmodified Gold Nanoparticles. *Biosens. Bioelectron.* **2010**, *25*, 1941−1946.
(10) Cai, M.; Li, F.; Zhang, Y.; Wang, Q. One-Pot Polymerase Chain Reaction with Gold Nanoparticles for Rapid and Ultrasensitive DNA Detection. *Nano Res.* **2010**, *3*, 557−563.
(11) Deng, H.; Xu, Y.; Liu, Y.; Che, Z.; Guo, H.; Shan, S.; Sun, Y.; Liu, X.; Huang, K.; Ma, X.; Wu, Y.; Liang, X.-J. Gold Nanoparticles with Asymmetric Polymerase Chain Reaction for Colorimetric Detection of DNA Sequence. *Anal. Chem.* **2012**, *84*, 1253−1258.
(12) Wong, J. K. F.; Yip, S. P.; Lee, T. M. H. Silica-Modified Oligonucleotide−Gold Nanoparticle Conjugate Enables Closed-Tube Colorimetric Polymerase Chain Reaction. *Small* **2012**, *8*, 214−219.
(13) Shen, W.; Deng, H.; Teo, A. K. L.; Gao, Z. Colorimetric Detection of Single-Nucleotide Polymorphisms with a Real-Time PCR-Like Sensitivity. *Chem. Commun.* **2012**, *48*, 10225−10227.
(14) Shen, W.; Deng, H.; Gao, Z. Gold Nanoparticle-Enabled Real-Time Ligation Chain Reaction for Ultrasensitive Detection of DNA. *J. Am. Chem. Soc.* **2012**, *134*, 14678−14681.
(15) Yin, H.; Huang, X.; Ma, W.; Xu, L.; Zhu, S.; Kuang, H.; Xu, C. Ligation Chain Reaction Based Gold Nanoparticle Assembly for Ultrasensitive DNA Detection. *Biosens. Bioelectron.* **2014**, *52*, 8−12.
(16) Kato, D.; Oishi, M. Ultrasensitive Detection of DNA and RNA Based on Enzyme-Free Click Chemical Ligation Chain Reaction on Dispersed Gold Nanoparticles. *ACS Nano* **2014**, *8*, 9988−9997.
(17) Valentini, P.; Pompa, P. P. A Universal Polymerase Chain Reaction Developer. *Angew. Chem., Int. Ed.* **2016**, *55*, 2157−2160.
(18) Tan, E.; Wong, J.; Nguyen, D.; Zhang, Y.; Erwin, B.; Van Ness, L. K.; Baker, S. M.; Galas, D. J.; Niemz, A. Isothermal DNA Amplification Coupled with DNA Nanosphere-Based Colorimetric Detection. *Anal. Chem.* **2005**, *77*, 7984−7992.
(19) Xu, W.; Xue, X.; Li, T.; Zeng, H.; Liu, X. Ultrasensitive and Selective Colorimetric DNA Detection by Nicking Endonuclease Assisted Nanoparticle Amplification. *Angew. Chem., Int. Ed.* **2009**, *48*, 6849−6852.
(20) Li, J.; Deng, T.; Chu, X.; Yang, R.; Jiang, J.; Shen, G.; Yu, R. Rolling Circle Amplification Combined with Gold Nanoparticle Aggregates for Highly Sensitive Identification of Single-Nucleotide Polymorphisms. *Anal. Chem.* **2010**, *82*, 2811−2816.
(21) Song, J.; Li, Z.; Cheng, Y.; Liu, C. Self-Aggregation of Oligonucleotide-Functionalized Gold Nanoparticles and Its Applications for Highly Sensitive Detection of DNA. *Chem. Commun.* **2010**, *46*, 5548−5550.
(22) Cui, L.; Ke, G.; Zhang, W. Y.; Yang, C. J. A Universal Platform for Sensitive and Selective Colorimetric DNA Detection Based on Exo III Assisted Signal Amplification. *Biosens. Bioelectron.* **2011**, *26*, 2796−2800.
(23) Xu, W.; Xie, X.; Li, D.; Yang, Z.; Li, T.; Liu, X. Ultrasensitive Colorimetric DNA Detection Using a Combination of Rolling Circle Amplification and Nicking Endonuclease-Assisted Nanoparticle Amplification (NEANA). *Small* **2012**, *8*, 1846−1850.
(24) Seetang-Nun, Y.; Jaroenram, W.; Sriurairatana, S.; Suebsing, R.; Kiatpathomchai, W. Visual Detection of White Spot Syndrome Virus Using DNA-Functionalized Gold Nanoparticles as Probes Combined with Loop-Mediated Isothermal Amplification. *Mol. Cell. Probes* **2013**, *27*, 71−79.
(25) Zhou, C.; Mu, Y.; Yang, M.-C.; Wu, Q.-Q.; Xu, W.; Zhang, Y.; Jin, W.; Song, Q.; Wu, Z.-Y.; Jin, Q.-H. Gold Nanoparticles Based Colorimetric Detection of Target DNA after Loop-Mediated Isothermal Amplification. *Chem. Res. Chin. Univ.* **2013**, *29*, 424−428.
(26) Valentini, P.; Fiammengo, R.; Sabella, S.; Gariboldi, M.; Maiorano, G.; Cingolani, R.; Pompa, P. P. Gold-Nanoparticle-Based Colorimetric Discrimination of Cancer-Related Point Mutations with Picomolar Sensitivity. *ACS Nano* **2013**, *7*, 5530−5538.
(27) Wong, J. K. F.; Yip, S. P.; Lee, T. M. H. Ultrasensitive and Closed-Tube Colorimetric Loop-Mediated Isothermal Amplification Assay Using Carboxyl-Modified Gold Nanoparticles. *Small* **2014**, *10*, 1495−1499.
(28) Wu, S.; Liang, P.; Yu, H.; Xu, X.; Liu, Y.; Lou, X.; Xiao, Y. Amplified Single Base-Pair Mismatch Detection via Aggregation of Exonulease-Sheared Gold Nanoparticles. *Anal. Chem.* **2014**, *86*, 3461−3467.
(29) Ma, C.; Wang, W.; Mulchandani, A.; Shi, C. A Simple Colorimetric DNA Detection by Target-Induced Hybridization Chain Reaction for Isothermal Signal Amplification. *Anal. Biochem.* **2014**, *457*, 19−23.
(30) Zou, B.; Cao, X.; Wu, H.; Song, Q.; Wang, J.; Kajiyama, T.; Kambara, H.; Zhou, G. Sensitive and Specific Colorimetric DNA Detection by Invasive Reaction Coupled with Nicking Endonuclease-Assisted Nanoparticles Amplification. *Biosens. Bioelectron.* **2015**, *66*, 50−54.
(31) Duan, R.; Wang, B.; Hong, F.; Zhang, T.; Jia, Y.; Huang, J.; Hakeem, A.; Liu, N.; Lou, X.; Xia, F. Real-Time Monitoring of Enzyme-Free Strand Displacement Cascades by Colorimetric Assays. *Nanoscale* **2015**, *7*, 5719−5725.
(32) Wen, J.; Chen, J.; Zhuang, L.; Zhou, S. Designed Diblock Hairpin Probes for the Nonenzymatic and Label-Free Detection of Nucleic Acid. *Biosens. Bioelectron.* **2016**, *79*, 656−660.
(33) Zhao, Y.; Chen, F.; Li, Q.; Wang, L.; Fan, C. Isothermal Amplification of Nucleic Acids. *Chem. Rev.* **2015**, *115*, 12491−12545.
(34) Notomi, T.; Okayama, H.; Masubuchi, H.; Yonekawa, T.; Watanabe, K.; Amino, N.; Hase, T. Loop-Mediated Isothermal Amplification of DNA. *Nucleic Acids Res.* **2000**, *28*, e63.
(35) Mori, Y.; Nagamine, K.; Tomita, N.; Notomi, T. Detection of Loop-Mediated Isothermal Amplification Reaction by Turbidity Derived from Magnesium Pyrophosphate Formation. *Biochem. Biophys. Res. Commun.* **2001**, *289*, 150−154.
(36) Nagamine, K.; Hase, T.; Notomi, T. Accelerated Reaction by Loop-Mediated Isothermal Amplification Using Loop Primers. *Mol. Cell. Probes* **2002**, *16*, 223−229.
(37) Frens, G. Controlled Nucleation for the Regulation of the Particle Size in Monodisperse Gold Suspensions. *Nature, Phys. Sci.* **1973**, *241*, 20−22.
(38) Grabar, K. C.; Freeman, R. G.; Hommer, M. B.; Natan, M. J. Preparation and Characterization of Au Colloid Monolayers. *Anal. Chem.* **1995**, *67*, 735−743.
(39) Haiss, W.; Thanh, N. T. K.; Aveyard, J.; Fernig, D. G. Determination of Size and Concentration of Gold Nanoparticles from UV−Vis Spectra. *Anal. Chem.* **2007**, *79*, 4215−4221.
(40) Chen, R. J.; Zhang, Y.; Wang, D.; Dai, H. Noncovalent Sidewall Functionalization of Single-Walled Carbon Nanotubes for Protein Immobilization. *J. Am. Chem. Soc.* **2001**, *123*, 3838−3839.
(41) Xu, Y.; Bai, H.; Lu, G.; Li, C.; Shi, G. Flexible Graphene Films via the Filtration of Water-Soluble Noncovalent Functionalized Graphene Sheets. *J. Am. Chem. Soc.* **2008**, *130*, 5856−5857.
(42) Van Leeuwen, Y. M.; Velikov, K. P.; Kegel, W. K. Morphology of Colloidal Metal Pyrophosphate Salts. *RSC Adv.* **2012**, *2*, 2534−2540.
(43) Kaneko, H.; Kawana, T.; Fukushima, E.; Suzutani, T. Tolerance of Loop-Mediated Isothermal Amplification to a Culture Medium and Biological Substances. *J. Biochem. Biophys. Methods* **2007**, *70*, 499−501.

DOI: 10.1021/acsami.7b00046
ACS Appl. Mater. Interfaces 2017, 9, 10472−10480

(44) Francois, P.; Tangomo, M.; Hibbs, J.; Bonetti, E.-J.; Boehme, C. C.; Notomi, T.; Perkins, M. D.; Schrenzel, J. Robustness of a Loop-Mediated Isothermal Amplification Reaction for Diagnostic Applications. *FEMS Immunol. Med. Microbiol.* **2011**, *62*, 41−48.

DOI: 10.1021/acsami.7b00046
ACS Appl. Mater. Interfaces 2017, 9, 10472−10480